ISSN 1674-1056
http://cpb.iphy.ac.cn
http://iopscience.iop.org/cpb
中国物理 B
Chinese Physics
中国物理
Chinese Physics B

Observation of geometric phase in a dispersively coupled resonator-qutrit system

Libo Zhang(张礼博), Chao Song(宋超), H Wang(王浩华), Shi-Biao Zheng(郑仕标)

Citation: Chin. Phys. B . 2018, 27(7): 070303. **doi:** 10.1088/1674-1056/27/7/070303

Journal homepage: http://cpb.iphy.ac.cn; http://iopscience.iop.org/cpb

What follows is a list of articles you may be interested in

Speeding up transmissions of unknown quantum information along Ising-type quantum channels

W J Guo(郭伟杰), L F Wei(韦联福)

Chin. Phys. B . 2017, 26(1): 010303. **doi:** 10.1088/1674-1056/26/1/010303

Design of a gap tunable flux qubit with FastHenry

Naheed Akhtar, Yarui Zheng(郑亚锐), Mudassar Nazir, Yulin Wu(吴玉林), Hui Deng(邓辉), Dongning Zheng(郑东宁), Xiaobo Zhu(朱晓波)

Chin. Phys. B . 2016, 25(12): 120305. **doi:** 10.1088/1674-1056/25/12/120305

A method for generating double-ring-shaped vector beams

Huan Chen(陈欢), Xiao-Hui Ling(凌晓辉), Zhi-Hong Chen(陈知红), Qian-Guang Li(李钱光), Hao Lv(吕昊), Hua-Qing Yu(余华清), Xu-Nong Yi(易煦农)

Chin. Phys. B . 2016, 25(7): 074201. **doi:** 10.1088/1674-1056/25/7/074201

Induced modification of geometric phase of a qubit coupled to an XY spin chain by the Dzyaloshinsky–Moriya interaction

Zhang Ai-Ping, Li Fu-Li

Chin. Phys. B . 2013, 22(3): 030308. **doi:** 10.1088/1674-1056/22/3/030308

Quantum communication via controlled holes in the statistical distribution of excitations in a nanoresonator coupled to a Cooper pair box

C. Valverde,A.T. Avelar,B. Baseia

Chin. Phys. B . 2012, 21(3): 030308. **doi:** 10.1088/1674-1056/21/3/030308

RAPID COMMUNICATION

Observation of geometric phase in a dispersively coupled resonator-qutrit system*

Libo Zhang(张礼博)[1], Chao Song(宋超)[1], H Wang(王浩华)[1,†], and Shi-Biao Zheng(郑仕标)[2,‡]

[1] Department of Physics, Zhejiang University, Hangzhou 310027, China

[2] Fujian Key Laboratory of Quantum Information and Quantum Optics, College of Physics and Information Engineering, Fuzhou University, Fuzhou 350116, China

(Received 4 March 2018; revised manuscript received 26 April 2018; published online 25 June 2018)

We present an experiment of observing the geometric phase in a superconducting circuit where the resonator and the qutrit energy levels are dispersively coupled. The drive applied to the resonator displaces its state components associated with the qutrit's ground state and first-excited state along different circular trajectories in phase space. We identify the resonator's phase-space trajectories by Wigner tomography using an ancilla qubit, following which we observe the difference between the geometric phases associated with these trajectories using Ramsey interferometry. This geometric phase is further used to construct the single-qubit π-phase gate with a process fidelity of 0.851 ± 0.001.

Keywords: geometric phase, superconducting circuit, Wigner tomography

PACS: 03.65.Vf, 03.67.Lx, 42.50.Pq **DOI:** 10.1088/1674-1056/27/7/070303

1. Introduction

A quantum system moving cyclically in its quantum-state space acquires a geometric phase that is proportional to the area enclosed by the cyclic path.[1,2] Since the magnitude of the geometric phase is only determined by the total area enclosed, local deformations of the path due to noise perturbations have minimal impact on the overall geometric phase acquired. This unique property offers a favorable choice for noise-resilient coherent manipulation of quantum states and for realization of high-fidelity quantum gates.[3–11] The geometric phase has been experimentally observed in various quantum systems,[12–21] and its noise resilience has been investigated.[17,18]

In a recent experiment,[22] a continuous-variable geometric phase has been utilized to implement a highly efficient quantum gate protocol in a superconducting circuit, where the resonator frequency and the qutrit $|e\rangle \leftrightarrow |f\rangle$ transition frequency ω_e are quasi-resonant. Here $|g\rangle$, $|e\rangle$, and $|f\rangle$ denote the ground, the first-excited, and the second-excited states of the qutrit, respectively. The geometric phase is due to the resonator motion in its phase space under an off-resonant microwave drive, which is present only when the qutrit is in $|g\rangle$. However, the quasi-resonance requirement is quite stringent since it restricts the spectrum width within which the qutrits can be placed, i.e., the qutrit $|e\rangle \leftrightarrow |f\rangle$ transition must be placed very close to the resonator in frequency. For non-tunable qutrits where the qutrit frequencies are fixed during the device design and fabrication process,[23] the protocol in Ref. [22] is impossible to be implemented.

Here we present an alternative experiment, with less strict requirements, for observing the geometric phase while the resonator can be dispersively coupled to the qutrit $|g\rangle \leftrightarrow |e\rangle$ and $|e\rangle \leftrightarrow |f\rangle$ transitions. The resonator's state components associated with $|g\rangle$ and $|e\rangle$ are moved along different loops in phase space, each accumulating a geometric phase proportional to the area enclosed by the corresponding loop. The geometric phase is determined by the difference of the areas enclosed by the two paths. We identify the resonator's phase-space trajectories by Wigner tomography using an ancilla qubit, following which we demonstrate the associated geometric phase with Ramsey interferometry. The experimental results are compared with the numerical simulations with good agreement. We further use this geometric phase to construct the single-qubit π-phase gate with a quantum process fidelity of 0.851 ± 0.001.

2. Experimental design

Our device, shown in Fig. 1(a), consists of a half-wavelength coplanar waveguide resonator coupled to two Xmon qutrits,[24,25] one serving as the test in Ramsey interferometry to read out the geometric phase and the second one used as an ancilla for Wigner tomography of the resonator. The two Xmon qutrits have weak anharmonicities $\eta = \omega_g - \omega_e \approx 2\pi \times 230$ MHz, and their $|g\rangle \leftrightarrow |e\rangle$ transitions are cou-

*Project supported by the National Basic Research Program of China (Grant No. 2014CB921201) and the National Natural Science Foundation of China (Grant Nos. 11434008 and 11574380).

†Corresponding author. E-mail: hhwang@zju.edu.cn

‡Corresponding author. E-mail: t96034@fzu.edu.cn

© 2018 Chinese Physical Society and IOP Publishing Ltd

pled to the resonator with coupling strengths $\lambda/2\pi \approx 23$ MHz, where ω_g is the $|g\rangle \leftrightarrow |e\rangle$ transition frequency.[26] The resonator has a fixed bare resonant frequency $\omega_c/2\pi$, which is estimated to be 5.042 GHz if the resonator is ideally decoupled from the test qutrit. Each qutrit can be dispersively or resonantly coupled to the resonator by tuning its frequency, and the coupling is effectively switched off when the qutrit is far off-resonant with the resonator. The Xmon qutrits can be treated as two-level qubits if their $|f\rangle$ levels play negligible roles at certain experimental stages. For example, the ancilla qutrit is set at $\omega_e/2\pi = 4.799$ GHz and is used as a qubit for Wigner tomography. In Ref. [22], the detuning between the bare resonator and the test qutrit is set to $|\omega_e - \omega_c| \approx \lambda$, while here we set $|\omega_g - \omega_c| \gg \lambda$. At the noted frequency, the $|e\rangle$-state lifetime of the test qutrit is measured to be around 9 μs, while the Gaussian dephasing time is around 1 μs.[27]

The dispersive resonator–qutrit coupling results in a frequency shift of the resonator that is dependent upon the state of the test qutrit, so that the resonator-drive detuning is also qutrit-state dependent, as shown in Fig. 1(b). The Hamiltonian describing the resonator's conditional frequency shift in the framework rotating at the drive frequency ω_d is

$$H/\hbar = (-\delta_d + \delta_g |g\rangle\langle g| + \delta_e |e\rangle\langle e|) a^\dagger a + \Omega\left(a + a^\dagger\right), \quad (1)$$

where $a^\dagger$ and a are the creation and annihilation operators of the resonator, Ω is the microwave drive amplitude, δ_d is the detuning between the drive and the bare resonator (without coupling to the qutrit), and δ_g (δ_e) is the resonator frequency shift associated with the qutrit state $|g\rangle$ ($|e\rangle$). We note that, for the quasi-resonant case where the resonator frequency and the qutrit $|e\rangle \leftrightarrow |f\rangle$ transition frequency ω_e are close, defining $\delta = \delta_d - \delta_g$, the δ_e term in Eq. (1) vanishes and the equation would take the same form as the Hamiltonian used in Ref. [22]. Here defining $\Delta_j = \delta_d - \delta_j$, where $j = g$ or e, the resulting evolution operator under the Hamiltonian H is

$$U_j(t) = \sum_{j=g,e} e^{i\Theta_j} e^{i\Delta_j a^\dagger a t} D[\alpha_j(t)] |j\rangle\langle j|, \quad (2)$$

where

$$\Theta_j = -\frac{\Omega^2}{\Delta_j}\left[t - \frac{1}{\Delta_j}\sin(\Delta_j t)\right],$$

and

$$D[\alpha_j(t)] = \exp\left[\alpha_j(t) a^\dagger - \alpha_j^*(t) a\right]$$

is the resonator's displacement operator, with $\alpha_j(t) = \int_0^t -i\Omega e^{i\Delta_j t}\,dt = \frac{\Omega}{\Delta_j}(1 - e^{-i\Delta_j t})$.

For the resonator that is initialized in the vacuum state $|0\rangle$ and subject to the drive Ω, it is displaced along a circular loop in phase space with the radium Ω/Δ_j and the angular velocity Δ_j depending upon the qutrit state $|j\rangle$, as shown in Fig. 1(c). When the qutrit is in the state $|j\rangle$, at time $T = 2k_j\pi/\Delta_j$ with k_j being an integer, the resonator returns back to $|0\rangle$ after k_j cycles in evolution, acquiring an Aharonov–Anandan phase $\Theta_j = -2k_j A_j$, where $A_j = \pi(\Omega/\Delta_j)^2$ is the area enclosed by the resonator's phase-space loop associated with the qutrit state $|j\rangle$. When $T = 2k_g\pi/\Delta_g = 2k_e\pi/\Delta_e$ with k_g and k_e both being integers, the resonator returns to $|0\rangle$ after the cyclic evolution no matter whether the qutrit is in the state $|g\rangle$ or $|e\rangle$; the two subsystems are disentangled even for an initial qutrit superposition state. As a result, the geometric phase acquired by the resonator depends on the qutrit state.

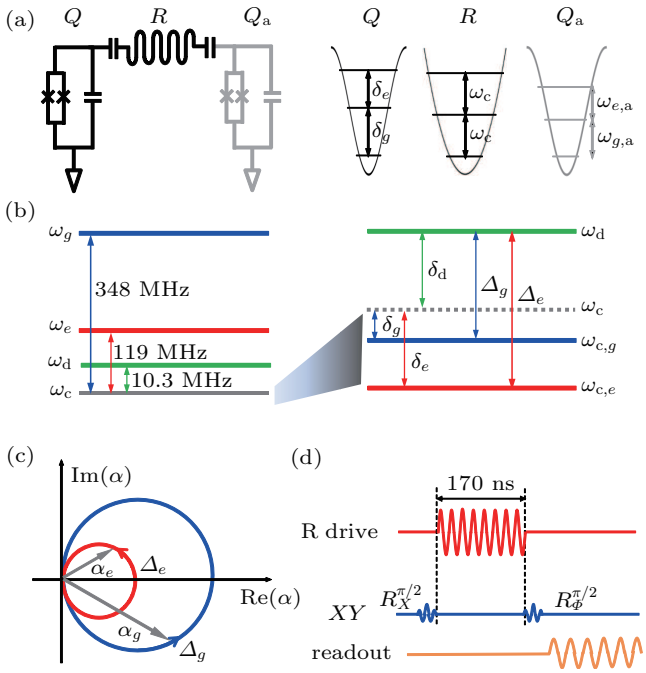


Fig. 1. (color online) Experimental layout. (a) Device schematic showing two Xmon qutrits coupled to a resonator in the middle (left), and the corresponding potential-well landscapes and energy levels (right). (b) Energy level arrangement of the resonator and the test qutrit ignoring their interaction (left), and the resonator's conditional frequency shifts due to the qutrit's dispersion (right). The microwave drive with a tone ω_d is detuned from ω_c by an amount δ_d. The dispersive coupling to the qutrit shifts the resonator frequency by an amount δ_g (δ_e), and hence the effective drive-resonator detuning is $\Delta_g \equiv \omega_d - \omega_{c,g} = \delta_d - \delta_g$ ($\Delta_e \equiv \omega_d - \omega_{c,e} = \delta_d - \delta_e$) for the qutrit state $|g\rangle$ ($|e\rangle$). (c) Ideal resonator's phase-space trajectories. The resonator, initially in its vacuum state, is displaced by the microwave drive along a circular loop in its phase space with the radium Ω/Δ_g (Ω/Δ_e) and the angular velocity Δ_g (Δ_e) for the qutrit state $|g\rangle$ ($|e\rangle$), where Ω is the drive amplitude. When the resonator traverses the loop once, it will acquire a geometric phase that is proportional to the enclosed phase-space area. When $\Delta_g/\Delta_e = k_g/k_e$, with k_g and k_e being integers, at time $T = 2\pi(k_g - k_e)/(\Delta_g - \Delta_e)$ the resonator makes a cyclic evolution and returns to the vacuum state no matter whether the qutrit is in the state $|g\rangle$ or $|e\rangle$; however, it acquires different geometric phases for these two qutrit states. (d) Ramsey sequence. The geometric operation, which is achieved by the combination of the microwave driving pulse (red sinusoid) and the dispersive resonator-qubit coupling, is sandwiched in between two $\pi/2$ qubit rotations (blue sinusoids) whose rotation axes differ by an angle Φ. The geometric phase difference β is manifested in the test qubit's Ramsey interference, obtained by a dispersive measurement using a 700 ns-long microwave pulse (light brown sinusoid).

Figure 2(a) displays the exemplary resonator's phase-space trajectories for the test qutrit in $|g\rangle$ and $|e\rangle$ as mapped out by Wigner tomography using the ancilla,[28] with the relevant

experimental parameters listed in Table 1. In Wigner tomography, the resonator state is described by a complex number α, where $|\alpha|^2$ represents the average photon number stored in the resonator.[29] The apparent agreement between the experimental data in Fig. 2(a) and the theory in Fig. 1(c) indicates the existence of the geometric phases when the resonator, dressed by the test qutrit states, is off-resonantly driven. We further use the test qutrit's $|g\rangle \leftrightarrow |e\rangle$ Ramsey interference to detect the geometric phase,[19,30,31] where the $|f\rangle$ state is not participating so that the test qutrit can now be treated as a two-level qubit. The pulse sequence for the Ramsey experiment shown in Fig. 1(d) starts by applying a $\pi/2$ pulse that rotates the qubit around the x-axis on the Bloch sphere, transforming the state of the qubit from $|g\rangle$ to $\frac{1}{\sqrt{2}}(|g\rangle - \mathrm{i}\,|e\rangle)$. Then the resonator is driven by a microwave pulse with a tone ω_d and an amplitude Ω for a duration $T \approx 170$ ns. ω_d and hence δ_d can be adjusted so that $\Delta_g/\Delta_e \approx k_g/k_e$, as shown in Table 1. We first choose $\delta_\mathrm{d}/2\pi = 10.3$ MHz, so that $k_g \simeq 2$ and $k_e \simeq 3$, and the qubit is approximately disentangled with the resonator at the end of this pulse, yielding the qubit state $\frac{1}{\sqrt{2}}\left(|g\rangle - \mathrm{i}\,\mathrm{e}^{\mathrm{i}\beta}\,|e\rangle\right)$, where $\beta = \Theta_e - \Theta_g$ is the geometric phase difference associated with the resonator's cyclic evolutions. A second $\pi/2$ rotation, around the axis with an angle Φ to the x-axis in the x–y plane, is then applied to the qubit, leading to the state

$$\frac{1}{2}\left\{\left[1-\mathrm{e}^{\mathrm{i}(\beta-\Phi)}\right]|g\rangle - \mathrm{i}\,\mathrm{e}^{\mathrm{i}\Phi}\left[1+\mathrm{e}^{\mathrm{i}(\beta-\Phi)}\right]|e\rangle\right\}. \quad (3)$$

Finally, the qubit is detected, with the probability of being measured in the excited state

$$P_e = \frac{1}{2}\left[1+\cos(\beta-\Phi)\right]. \quad (4)$$

Table 1. Choices of the drive frequency for realizing the resonator's cyclic evolution while maintaining k_g and k_e both integers.

$(\delta_\mathrm{d}/2\pi)$/MHz	$(\Delta_g/2\pi)$/MHz	$(\Delta_e/2\pi)$/MHz	k_g/k_e
10.3	11.9	18.0	2/3
16.2	17.8	23.9	3/4
22.2	23.8	29.9	4/5

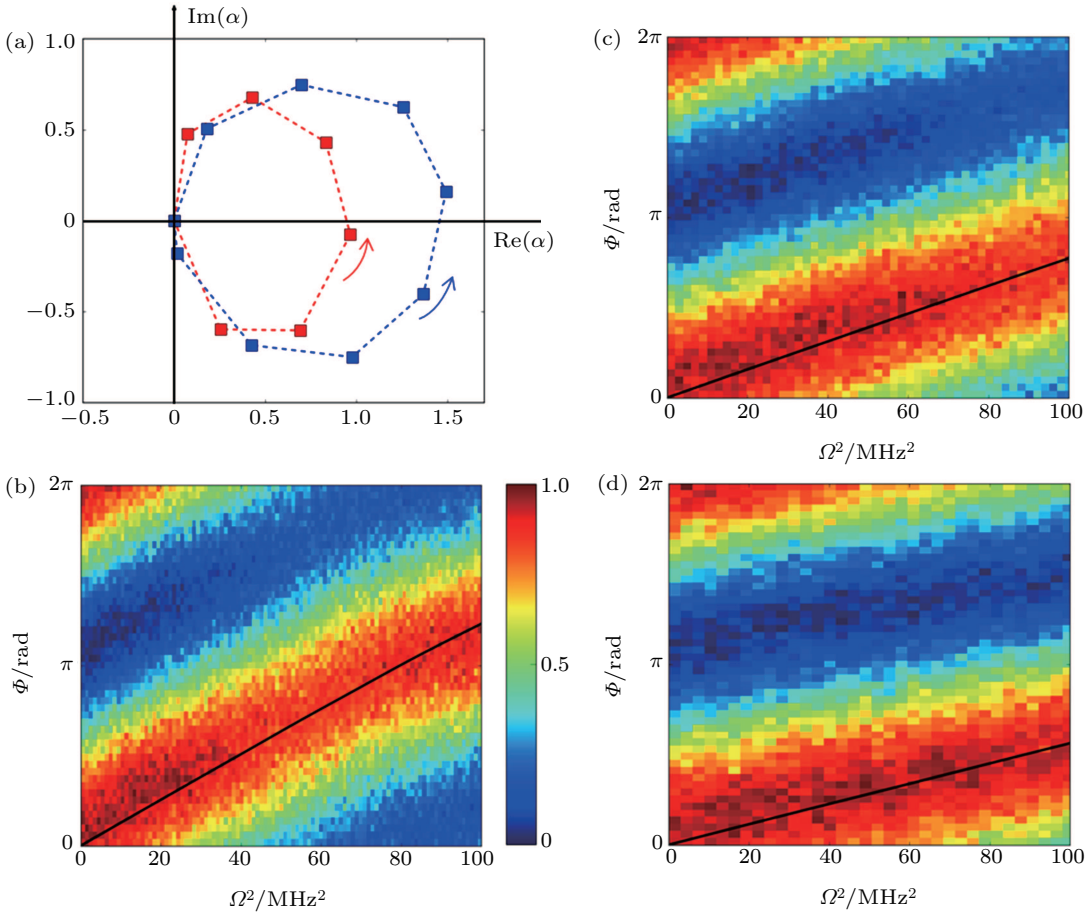


Fig. 2. (color online) Geometric phase. (a) Exemplary resonator's phase-space trajectories for the test qutrit in $|g\rangle$ (blue squares) and $|e\rangle$ (red squares) by sampling at a few selected time intervals during the evolutions with Wigner tomography using the ancilla.[28] Some relevant experimental parameters are $\Omega/2\pi \approx \sqrt{91}$ MHz, $\delta_\mathrm{d}/2\pi = 10.3$ MHz, $\Delta_g/2\pi = 11.9$ MHz, and $\Delta_e/2\pi = 18.0$ MHz. Dashed lines are visual guides connecting the experimental data points. (b)–(d) Ramsey interferences: probabilities P_e of the test qubit in the excited state $|e\rangle$, with color bar in (b), as functions of Φ and Ω^2 for $\delta_\mathrm{d}/2\pi = 10.3$ MHz (b), $\delta_\mathrm{d}/2\pi = 11.6$ MHz (c), and $\delta_\mathrm{d}/2\pi = 22.2$ MHz (d), with $T \approx 170$ ns. Other relevant parameters can be found in Table 1. Solid lines are numerical simulations for the dispersively coupled resonator–test qutrit system with the assumption of an extra driving strength of 0.3Ω to the test qutrit in the full Hamiltonian due to the on-chip microwave crosstalk. For a fixed P_e, the linear scaling of Φ with Ω^2 is clearly observed, which, according to Eq. (4), implies that the geometric phase difference β is also linear in Ω^2.

Equation (4) shows that P_e remains unchanged when β and Φ are varied by the same amount. In Fig. 2(b), we present the measured P_e as a function of Φ and Ω^2, which shows that, for a fixed P_e, Φ and hence β are linear in Ω^2 that is proportional to the phase-space area enclosed by each loop. Equation (4) shows that if and only if $\beta = \Phi$, we have $P_e = 1$, based on which we can directly obtain β as a function of Ω^2 by tracing the contour of P_e maximum in Fig. 2(b). Excellent agreement with the numerical solution (solid line) for the data in Fig. 2(b) verifies the linear scaling of β with the difference between the areas swept by the coherent states $|\alpha_j(t)\rangle$ associated with $j = |g\rangle$ and $|e\rangle$. As also verified by the numerical simulation, the total phase observed in Fig. 2(b) contains a dynamical contribution which is proportional to Ω^2 as well, since the test qutrit is driven through the microwave crosstalk during the evolutions.

Figures 2(c) and 2(d) display the measured P_e versus Φ and Ω^2 for another two choices of the drive frequency δ_d (Table 1), all for the pulse duration of $T \approx 170$ ns. As expected, in each case the measured geometric phase difference β, which is equal to Φ for $P_e = 1$, shows the similar linear scaling with Ω^2. When Φ and Ω are fixed, the observed geometric phase difference decreases with increasing δ_d. This can be explained as follows. The acquired geometric phase is proportional to the product of the area enclosed by the phase-space circle and the number of turns in the pulse duration. The area decreases quadratically with the increase of the drive-resonator detuning as $A_j = \pi(\Omega/\Delta_j)^2$, while for a fixed pulse duration, the cyclic number scales linearly with the detuning.

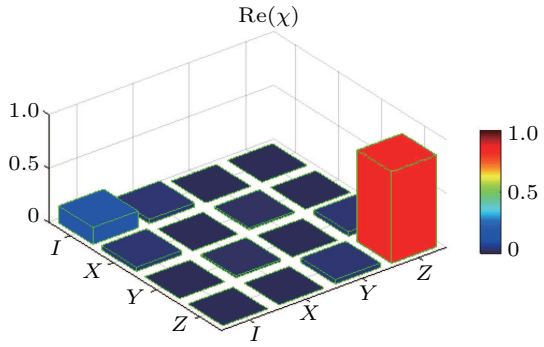


Fig. 3. (color online) Geometric π-phase gate, which is performed in a separate experiment on a similar device, with $\Omega/2\pi \approx \sqrt{133}$ MHz, $\delta_d/2\pi = 17.1$ MHz, $\Delta_g/2\pi = 12.5$ MHz, $\Delta_e/2\pi = 18.8$ MHz, and $T \approx 160$ ns. Real part of the QPT matrix, χ, for the π-phase geometric gate is expressed in the Pauli basis $\{I, X, Y, Z\}$, with a process fidelity of about 0.851 ± 0.001.

As shown above, the geometric phase of the resonator is encoded in the final state of the test qubit, i.e., the $|g\rangle \leftrightarrow |e\rangle$ transition of the test qutrit, producing a geometric phase gate on the qubit. In order to characterize this gate, we carry out quantum process tomography (QPT) in a separate experiment on a similar device, where the same geometric phase has been observed. In this device, the test qutrit's $|g\rangle \leftrightarrow |e\rangle$ transition frequency is 4.945 GHz, with a lifetime of around 17 μs and a Gaussian dephasing time of around 2 μs. The resonator frequency is 5.041 GHz, and the qutrit–resonator coupling strength is around 20 MHz. The π-phase gate with the choice of $\Omega/2\pi \approx \sqrt{133}$ MHz and $\delta_d/2\pi = 17.1$ MHz is characterized by QPT, and the QPT matrix is displayed in Fig. 3, with a process fidelity of 0.851 ± 0.001. This result demonstrates that the geometric phase can be used to realize quantum logic gates in superconducting circuits.

We note that our experimentally achieved fidelity value of the π-phase gate, which agrees well with the numerical simulation, is mostly determined by the device and measurement parameters including the qubit-resonator detuning $\omega_g - \omega_c$, the qubit-resonator coupling λ, and the qubit anharmonicity η. Further improvement is possible by increasing $|\omega_g - \omega_c|$, λ, and η appropriately, so that the difference between the qubit-state dependent resonator frequency shifts δ_e and δ_g can be improved, and the resonator's evolutions associated with the qubit states $|g\rangle$ and $|e\rangle$ can be simultaneously resynchronized with the drive after a shorter duration. For example, setting $(\omega_g - \omega_c)/2\pi = -800$ MHz, $\lambda/2\pi = 80$ MHz, and $\eta/2\pi = 500$ MHz, the numerical simulation indicates that the π-phase gate fidelity can be well above 0.99 ignoring decoherence. In addition, the geometric phase is advantageous for implementing a two-qubit controlled phase gate, as investigated in Refs. [23] and [32], where the geometric phase due to the resonator's cyclic motion in the phase space, though not directly observed via Ramsey interference, has been used to construct the resonator-induced two-qubit phase gate with fidelity up to 0.98.

3. Summary

In conclusion, we have carried out an alternative experiment for observation of the geometric phase of a harmonic oscillator in a superconducting circuit, which does not require the qutrit $|e\rangle \leftrightarrow |f\rangle$ transition to be close to the resonator in frequency. The difference between the geometric phases associated with the two traversed phase-space loops, which correlate with the qutrit states $|g\rangle$ and $|e\rangle$, is measured with a qubit-based Ramsey interferometer. Finally, the acquired geometric phase of the resonator can be used to produce the π-phase gate on the qubit with a gate fidelity of 0.851 ± 0.001 as characterized by quantum process tomography.

References

[1] Anandan J 1992 *Nature* **360** 307
[2] Aharonov Y and Anandan J 1987 *Phys. Rev. Lett.* **58** 1593
[3] Zanardi P and Rasetti M 1999 *Phys. Lett. A* **264** 94
[4] Jones J A, Vedral V, Ekert A and Castagnoli G 2000 *Nature* **403** 869
[5] Falci G, Fazio R, Palma G M, Siewert J and Vedral V 2000 *Nature* **407** 355
[6] Duan L M, Cirac J I and Zoller P 2001 *Science* **292** 1695

[7] Wang X B and Keiji M 2001 *Phys. Rev. Lett.* **87** 097901
[8] Zhu S L and Wang Z D 2002 *Phys. Rev. Lett.* **89** 097902
[9] Leibfried D, DeMarco B, Meyer V, Lucas D, Barrett M, Britton J, Itano W M, Jelenkovic B, Langer C, Rosenband T and Winel D J 2003 *Nature* **422** 412
[10] Zheng S B 2004 *Phys. Rev. A* **70** 052320
[11] Sjöqvist E, Tong D M, Andersson L M, Hessmo B, Johansson M and Singh K 2012 *New J. Phys.* **14** 103035
[12] Samuel J and Bhandari R 1988 *Phys. Rev. Lett.* **60** 2339
[13] Tycko R 1987 *Phys. Rev. Lett.* **58** 2281
[14] Suter D, Mueller K T and Pines A 1988 *Phys. Rev. Lett.* **60** 1218
[15] Webb C L, Godun R M, Summy G S, Oberthaler M K, Featonby P D, Foot C J and Burnett K 1999 *Phys. Rev. A* **60** R1783
[16] Feng G, Xu G and Long G 2013 *Phys. Rev. Lett.* **110** 190501
[17] Leek P J, Fink J M, Blais A, Bianchetti R, Göppl M, Gambetta J M, Schuster D I, Frunzio L, Schoelkopf R J and Wallraff A 2007 *Science* **318** 1889
[18] Filipp S, Klepp J, Hasegawa Y, Plonka-Spehr C, Schmidt U, Geltenbort P and Rauch H 2009 *Phys. Rev. Lett.* **102** 030404
[19] Pechal M, Berger S, Abdumalikov A A Jr, Fink J M, Mlynek J A, Steffen L, Wallraff A and Filipp S 2012 *Phys. Rev. Lett.* **108** 170401
[20] Tan X, Zhang D, Zhang Z, Yu Y, Han S and Zhu S 2014 *Phys. Rev. Lett.* **112** 027001
[21] Zhou H, Li Z, Wang H, Chen H, Peng X and Du J 2016 *Chin. Phys. Lett.* **33** 060301
[22] Song C, Zheng S B, Zhang P, Xu K, Zhang L, Guo Q, Liu W, Xu D, Deng H, Huang K, Zheng D, Zhu X and Wang H 2017 *Nat. Commun.* **8** 1061
[23] Paik H, Mezzacapo A, Sandberg M, McClure D T, Abdo B, Córcoles A D, Dial O, Bogorin D F, Plourde B L T, Steffen M, Cross A W, Gambetta J M and Chow Jerry M 2016 *Phys. Rev. Lett.* **117** 250502
[24] Song C, Xu K, Liu W, Yang C, Zheng S B, Deng H, Xie Q, Huang K, Guo Q, Zhang L, Zhang P, Xu D, Zheng D, Zhu X, Wang H, Chen Y A, Lu C Y, Han S and Pan J W 2017 *Phys. Rev. Lett.* **119** 180511
[25] Gu X, Kockumb A F, Miranowicz A, Liu Y X and Nori F 2017 *Phys. Rep.* **718** 1
[26] Xu H K, Song C, Liu W Y, Xue G M, Su F F, Deng H, Tian Y, Zheng D N, Han S, Zhong Y P, Wang H, Liu Y and Zhao S P 2016 *Nat. Commun.* **7** 11018
[27] Zhong Y, Li C, Wang H and Chen Y 2013 *Chin. Phys. B* **22** 110313
[28] Wang H, Mariantoni M, Bialczak R C, Lenander M, Lucero E, Neeley M, O0Connell A D, Sank D, Weides M, Wenner J, Yamamoto T, Yin Y, Zhao J, Martinis John M and Cleland A N 2011 *Phys. Rev. Lett.* **106** 060401
[29] Zheng S B 2002 *Phys. Rev. A* **66** 060303
[30] Zheng S B 2012 *Phys. Rev. A* **85** 022128
[31] Vacanti G, Fazio R, Kim M S, Palma G M, Paternostro M and Vedral V 2012 *Phys. Rev. A* **85** 022129
[32] Cross A W and Gambetta J M 2015 *Phys. Rev. A* **91** 032325